Tunable heat transfer with smart nanofluids

Michele Bernardin, Federico Comitani, and Alberto Vailati*
Dipartimento di Fisica, Università degli Studi di Milano, via Celoria 16, 20133 Milano, Italy
(Received 7 February 2012; revised manuscript received 30 May 2012; published 26 June 2012)

Strongly thermophilic nanofluids are able to transfer either small or large quantities of heat when subjected to a stable temperature difference. We investigate the bistability diagram of the heat transferred by this class of nanofluids. We show that bistability can be exploited to obtain a controlled switching between a conductive and a convective regime of heat transfer, so as to achieve a controlled modulation of the heat flux.

DOI: 10.1103/PhysRevE.85.066321 PACS number(s): 44.25.+f, 44.10.+i, 65.80.−g

I. INTRODUCTION

Nanofluids are suspensions of nanoparticles with size ranging from a few nanometers up to hundreds of nanometers, dispersed in a carrier liquid. Their use as a heat-transfer medium has been widely investigated, due to the report of a significant increase of their thermal conductivity with respect to that of the carrier liquid, even in the case of diluted suspensions [1–6]. Further investigation showed that the change in thermal conductivity is accompanied by an enhancement of mass diffusion in nanofluids [7], a feature which has been interpreted as due to interfacial complexation [8]. The opportunity of affecting the distribution of nanoparticles by means of external fields has led recently to the investigation of smart nanofluids with tunable thermal properties [9,10].

A new impulse toward the development of smart nanofluids has been originated by the discovery of bistable heat transfer in suspensions of highly thermophilic nanoparticles [11]. In such samples, under the action of a stable temperature difference the heat transfer occurs either in a conductive or in a convective regime, depending on the initial distribution of the nanoparticles inside the carrier liquid. The heat flux in the conductive regime is significantly smaller than that in the convective one. This feature suggests that highly thermophilic nanofluids could be used as smart materials for the control of the heat transferred. However, the suitability of nanofluids for this task requires one to be able to achieve a controlled transition between the conductive and convective regime.

In this work we investigate the bistability diagram of highly thermophilic nanofluids, and we show that a proper selection of their concentration allows us to tune their bistable behavior so to achieve a controlled switching between the two heat-transfer regimes. The choice of the regime depends on the spatial distribution of the particles at the time when the heat-transfer process is started by the imposition of a temperature difference: in the presence of a stabilizing concentration profile the conductive regime is selected, while in the presence of an unstable concentration profile the convective regime is selected. We show that the transition from one regime to the other can be achieved by exploiting the thermophilic nature of the nanoparticles to alter their spatial distribution, without performing any mechanical manipulations of the sample. We investigate the conditions needed to achieve a controlled transition in a time as short as possible.

As usual in hydrodynamics, the temperature difference ΔT imposed to the liquid and the heat transferred Q are best expressed by using dimensionless variables, provided by the Rayleigh number $\mathrm{Ra} = \alpha g \Delta T h^3/(\nu D_T)$ and the Nusselt number $\mathrm{Nu} = Qh/(\chi \Delta T)$, respectively [12,13]. Here α is the thermal expansion coefficient of the liquid, g is the acceleration of gravity, h is the sample thickness, ν is the kinematic viscosity, D_T is the thermal diffusivity, and χ is the thermal conductivity. The Nusselt number Nu quantifies the heat transferred by the sample relative to the amount of heat that would be transferred by conduction only.

II. EXPERIMENTAL SETUP

The sample is a horizontal layer of a suspension of spherical silica particles (LUDOX TMA) with a diameter of 32 nm dispersed in water [14]. It is contained into a thermal gradient cell shown schematically in Fig. 1.

The sample (NF) is sandwiched between two 8 mm thick, 70 mm diameter, sapphire windows (SW) and is confined laterally by an O ring gasket (OR) with an internal diameter of 45.9 mm and cord diameter of 4.5 mm. Three Delrin® spacers (DS) keep the sapphire windows at a distance $h = 2.85$ mm. The cell is kept under compression by means of two Delrin® flanges (DF). Each sapphire window is in thermal contact with an annular thermoelectric device (TED) through an aluminum ring (AR). The TEDs allow one to transfer heat to and from two toroidal thermal reservoirs (TRs) connected to a water circulating bath kept at a constant temperature of 25 °C. The temperature of the sapphire windows is measured by two 100 kΩ negative temperature coefficient thermistors located at the surfaces of contact between the sapphire windows and the TEDs. The temperature of each sapphire window can be controlled independently by using a proportional integral derivative (PID) servocontrol implemented in LABVIEW on a dedicated personal computer. The servocontrols drive two programmable Kepco AB power supplies that drive the TEDs. The high thermal conductivity of sapphire, of the order of 35 W/(m K), allows us to achieve a temperature distribution uniform within about 3%. The utilization of annular TEDs determines the presence of a clear window with a diameter of 27 mm at the center of the cell. This aperture can be used to visualize the convective pattern by using a shadowgraph diagnostic technique.

*alberto.vailati@unimi.it

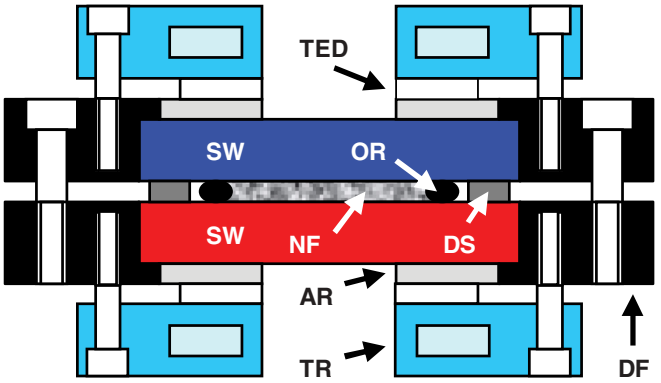

FIG. 1. (Color online) Scheme of the thermal gradient cell. The nanofluid NF is delimited horizontally by two sapphire windows SW and laterally by an O ring OR. The spacers DS keep the windows at a distance of 2.85 mm. The inner part of the cell is kept together by means of two flanges DF. The sapphire windows are in contact with two annular thermoelectric devices TED through two aluminum rings AR. Heat can be pumped from and to a water circulation loop TR connected to a thermostat.

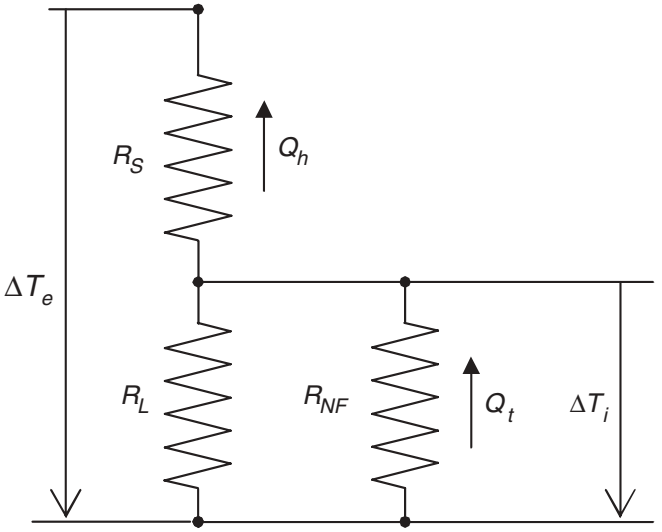

FIG. 2. Thermal modeling of the thermal gradient cell. A temperature difference ΔT_e is applied at the outer surfaces of the sapphire windows. As a consequence a heat Q_h flows through the cell. The sapphire windows act as a resistance R_S in series with the thermal resistance R_{NF} provided by the nanofluid. The flanges that keep the cell together act as a thermal resistance in parallel with the nanofluid. The network of thermal resistances acts as a voltage divider. As a consequence of the losses, the nanofluid is under the action of a temperature difference ΔT_i and is crossed by a heat flux Q_t.

III. CALIBRATION

The reliability and the performances of the Rayleigh-Bénard cell described here have been thoroughly checked during a long series of experiments performed by using cells sharing a common design [15–23].

The accurate measurement of the heat transferred by the sample requires to determine the amount of heat pumped by the TEDs. This is achieved by using the equations modeling the TEDs provided by the manufacturer [24]. As a reference, we consider the heat pumped by the TED at the bottom plate of the cell $Q_h = T_h S_M I + \frac{1}{2} I^2 R_M - K_M \Delta T_P$. Here I is the electric current flowing through the Peltier elements, S_M is the effective Seebeck coefficient, R_M is the electric resistance of the TED, K_M its thermal conductance, T_h is the temperature of the hot side of the TED, and ΔT_P is the temperature difference developed by the TED.

In order to measure the actual heat transferred by the sample layer under the action of a temperature difference we performed a careful calibration of the cell to achieve a quantitative characterization of heat losses due to parasitic heat conduction. The cell is modeled as a combination of thermal resistances, as shown in Fig. 2. The Peltier elements pump a known quantity of heat Q_h through the cell. The thermal resistance R_S determined by the sapphire windows is in series with the thermal resistance R_{NF} determined by the sample sandwiched between the sapphire windows. A thermal resistance R_L is added in parallel to R_{NF} to take into account the loss of the heat that flows into the cell structure. R_S and R_L are determined by performing two independent calibration measurements on reference samples of known thermal resistance sandwiched between the sapphire windows instead of the sample. As reference samples we used two Macor ceramics disks of diameter 50.0 mm and thickness 2.0 and 4.0 mm, respectively. Losses due to the presence of the O ring and of the spacers were measured independently by performing measurements of the heat transferred with an empty cell by heating from below. Under these conditions, the presence of air inside the cell determines an overestimation of the losses, which is accounted for by estimating the theoretical contribution to the heat transfer due to the convection of air and by subtracting it. The estimate of the losses due to the presence of the O ring and spacers is also checked for consistency by performing measurements by heating from above, a condition that prevents the onset of convection in the air trapped inside the cell.

The procedure outlined above allows us to obtain a reliable estimate of the heat flux Q_h through the cell and of the temperature difference ΔT_e that develops between the two surfaces of the sapphire windows in contact with the TED elements. The knowledge of R_S and R_L allows to determine the temperature difference ΔT_i falling on the sample and the heat Q_t flowing through it by using the usual equations for a voltage divider network: $Q_t = [Q_h (R_L + R_S) - \Delta T_e]/R_L$ and $\Delta T_i = \Delta T_e - Q_h R_S$.

The calibration has been checked by performing test measurements of the Nusselt number as a function of the Rayleigh number in pure water, shown by the green diamonds in Fig. 3. In the same figure we have also plotted for comparison high-accuracy data for liquid helium obtained by Behringer and Ahlers (crosses) [25]. Figure 3 shows that for a pure fluid below the threshold of Rayleigh-Bénard convection $\mathrm{Ra}_c = 1708$ the heat transfer takes place by conduction only, and $\mathrm{Nu} = 1$. Above this threshold convection sets in, and the heat transferred increases faster than it would do by conduction only.

IV. RESULTS

By adding a small amount of nanoparticles to water the bifurcation scenario changes dramatically [26–38]. The

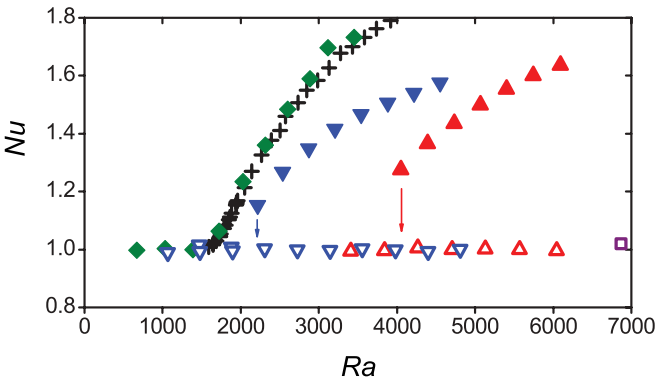

FIG. 3. (Color online) Nusselt number as a function of Rayleigh number. Diamonds represent results for pure water. Crosses are high-accuracy measurements on liquid helium [25]. Results for the LUDOX nanofluid at different concentration are shown by downwards triangles ($c = 2.0\%$), upwards triangles ($c = 4.0\%$), and squares ($c = 8.0\%$). Open and solid symbols correspond to heat transferred in the stable conductive and convective regimes, respectively. Arrows mark values of the Rayleigh number below which the conductive branch is no more stable and a spontaneous transition to the conductive regime occurs.

temperature gradient gives rise to a thermophoretic mass flux of particles $j = -\rho D[S_T c(1-c)\nabla T]$, where ρ is the density of the suspension, D is the diffusion coefficient of the nanoparticles into the carrier liquid, S_T the Soret coefficient, and c the weight fraction concentration of nanoparticles. Under steady flow conditions thermophoresis gives rise to a concentration difference Δc throughout the sample. Here we assume that the temperature and concentration gradients are directed vertically. The concentration difference is in turn associated with a density difference $\Delta\rho_c = \rho\beta\Delta c$, where $\beta = \rho^{-1}\partial\rho/\partial c$ is the solutal expansion coefficient. At the same time, the thermal dilation of the solution gives rise to a density difference $\Delta\rho_T$. The overall density variation from the top to the bottom of the sample can be written as the superposition of the two terms: $\Delta\rho = \Delta\rho_T + \Delta\rho_c$. The relative influence of the two terms on the stability of the nanofluid is expressed by the separation ratio $\Psi = \Delta\rho_c/\Delta\rho_T = \beta S_T c(1-c)/\alpha$. For the LUDOX sample under investigation in this work $\Psi = -89.0c(1-c)$ [14], and the particles move toward the warmer regions due to thermophoresis. The negative sign of Ψ indicates that in this case the two contributions have opposite effects on the stabilization and destabilization of the liquid layer.

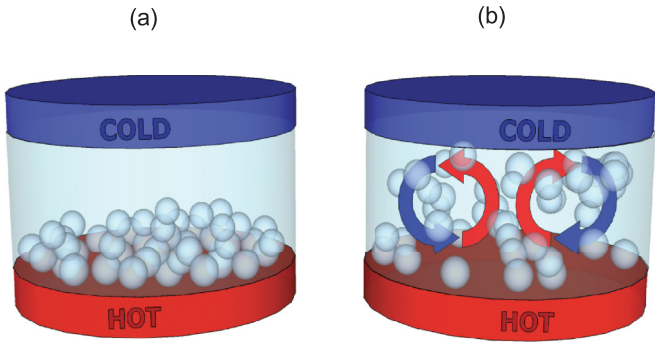

FIG. 4. (Color online) Sketch of the distribution of particles in the conductive and convective heat-transfer regimes. (a) In the conductive regime the strong thermophilic nature of the particles drives them toward the hot plate. This accumulation creates a stabilizing density profile, which prevents the onset of convective motions. (b) The convective regime is induced by dispersing the nanoparticles into the carrier liquid. The strong convective currents prevent the accumulation of particles at the hot plate, notwithstanding the flux of particles particle towards the hot plate induced by thermophoresis.

Under steady flow conditions the fact that $|\Psi| > 1$ means that the behavior of the sample is dominated by $\Delta\rho_c$. This suggests the opportunity of using the thermophoretic flux to alter the distribution of the particles inside the nanofluid, so to attain a controlled switching between the conductive and convective heat-transfer regimes. The heat transfer emerges from the dynamical competition between the destabilizing effect of the convective heat flux and the stabilizing action of the Soret flux of nanoparticles. The ratio between the time scales associated with the conductive transfer of heat and the diffusive transfer of nanoparticles is represented by the Lewis number $\mathrm{Le} = D_T/D$. For the nanofluid investigated in this work $\mathrm{Le} = 6.49 \times 10^3$. Such a large value of Le implies that the temperature profile inside the fluid can be changed almost instantaneously, without altering significantly the distribution of the nanoparticles during the process.

The sample is brought in a conductive state by slowly increasing the temperature difference by heating from below. In this way, the thermophoretic accumulation of the particles at the bottom plate creates a stabilizing boundary layer that prevents the onset of Rayleigh-Bénard convection, even at Rayleigh numbers well above the threshold $\mathrm{Ra}_c = 1708$ [Fig. 4(a)]. The temperature difference is increased by 1 K every 5 h. During this process the sample always remains on the conductive branch of the bistability diagram (Nu = 1; Fig. 3, open triangles).

In order to bring the sample from the conductive to the convective regime we devised a procedure that allows us to get rid of the particles accumulated at the bottom plate, which prevents the onset of the instability. This is achieved by temporarily reversing the temperature difference for about 2 h. In this way, the sample is heated from above, and the particles get accumulated at the top plate due to thermophoresis. This gives rise to the onset of a solutal convective instability in the nanofluid [17–19,21,22,39,40]. The large Lewis number of the nanofluid implies that the temperature field is uncoupled from the fluid velocity. This is due to the fact that the velocity of the solutal convective flux is very small. Therefore, the convective currents do not contribute effectively to the transfer of heat. As a result, the temperature profile is stabilizing, and the heat transfer occurs by conduction. By quickly reversing the temperature difference the sample is then brought back into the condition where it is heated from below and convection starts. This procedure prevents the particles from being accumulated at the bottom when Rayleigh-Bénard convection starts [Fig. 4(b)] and relies on the fact that the equilibration time of the temperature profile across the sample is of the order of 100 s, about two orders of magnitude smaller than the diffusive time needed to alter the distribution of particles at the boundaries.

The convective patterns are initially stationary. Then, after some of the particles migrate at the bottom boundary by thermophoresis, propagating waves appear, and this oscillatory convective regime lasts indefinitely.

Once that the sample was brought into the convective regime at a Rayleigh number of the order of 6000 the temperature difference was decreased stepwise (1 K every 10 h), and the Nusselt number was measured at every step. Data obtained by applying this procedure to the nanofluid are shown in Fig. 3. Full upwards triangles represent data taken at $c = 2.0\%$ ($\Psi = -1.74$), and full downwards triangles at $c = 4.0\%$ ($\Psi = -3.42$). We have not been able to bring the $c = 8.0\%$ ($\Psi = -6.55$) sample into a stable convective state, due to the very strong stabilizing action of the particles against convection at this concentration. From Fig. 3 one can appreciate how at the 4% concentration the strong stabilization generated by the thermophoretic accumulation of the particles at the bottom results in a lowering of the convective branch of the bistability diagram obtained for the 2% concentration.

This procedure for the destabilization of the sample differs significantly from that described in a previous paper [11], where the sample was destabilized by starting from a condition where the particle were distributed nearly uniformly inside the sample. The former procedure was aimed at obtaining a well-controlled initial condition at the cost of a very long time (of the order of 10 days) to collect a single experimental point of the stability curve. The controlled initial conditions allowed to estimate reliably the threshold Ra^* between transient convection and permanent oscillatory convection. The procedure adopted in this paper is aimed at assessing the best operating conditions to achieve a fast switching between the conductive and convective heat-transfer regimes. The destabilization of the sample exploiting the presence of a solutal instability gives rise to an initial condition dramatically different from the uniform concentration of nanoparticles adopted in the previous paper. We have collected experimental evidence that the stability curves are strongly influenced by the initial distribution of nanoparticles. In retrospect this results is reasonable, considered that the heat-transfer process involves the dynamic competition between the destabilizing action of the convective flux and the stabilizing action of the Soret flux. Therefore, the strong dependence from the initial condition prevents a comparison between the Rayleigh numbers corresponding to the transition from the convective to the conductive regime, indicated by the arrows in Fig. 3, and the Rayleigh numbers Ra^* previously reported in Ref. [11].

To establish the general character of the bistability phenomenon, we have investigated the opportunity to achieve a controlled switching between the conductive and convective heat-transfer regimes by using samples of different composition. The samples of choice are LUDOX TMA at a concentration $c = 2\%$, and HYFLON MFA at $c = 4.0\%$ ($\Psi = -7.5$) [14,41]. The LUDOX sample was subjected to a temperature difference $\Delta T = 9.6$ K (Ra = 5200), while for HYFLON $\Delta T = 11.5$ K (Ra = 4990). Both samples were first brought into a solutal convective regime by heating them from above for 2 h at $\Delta T = -20$ K. (Ra = −10 840 for the LUDOX sample and Ra = −8640 for the Hyflon one.) This determined

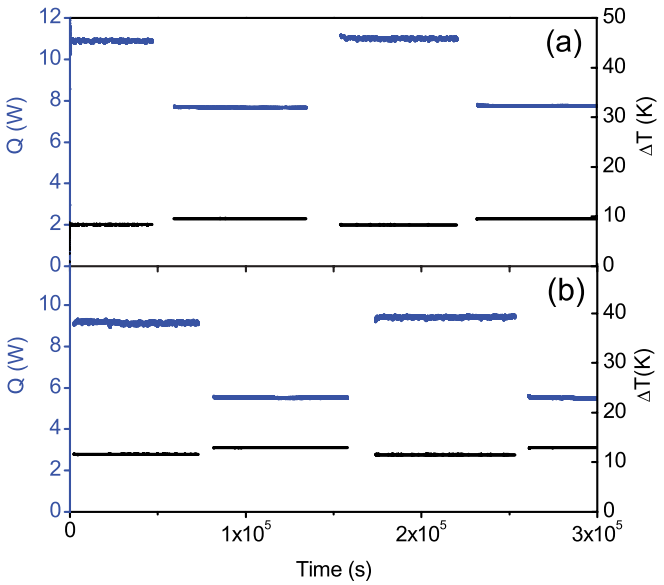

FIG. 5. (Color online) Plot of the heat transferred by the nanofluid (top) and temperature difference imposed to it (bottom) as a function of time. Panel a corresponds to LUDOX and panel b to HYFLON.

an unstable concentration profile where the nanoparticles are accumulated at the top of the cell. The temperature difference was then suddenly reversed, and the convective heat transfer started. The transition to the conductive regime was obtained by bringing the temperature difference below threshold and by imposing a slow ramp in the temperature difference, so that it reached a final value equal to that used in the convective regime in about one hour. The transition between the conductive and convective regimes was then iterated to assess the repeatability of the process. After each transition the sample was left in the conductive and convective state for a time in the range 16–22 h to assess the stability of the regime.

The results of these measurements are shown in Fig. 5(a) (LUDOX) and 5(b) (HYFLON). The typical increase in the heat flux in the transition from the conductive to the convective regime amounts to 41% for LUDOX and 75% for HYFLON, where the conductive heat fluxes are of the order of 4900 W/m^2 for LUDOX and 3500 W/m^2 for HYFLON. The tuning of the transition times showed that a reliable transition can be achieved in times of the order of 9,000–16,000 s. Much smaller times do not allow a reliable transition between the two regimes.

Our results show that the utilization of highly thermophilic particles allows us to achieve an active control of the heat transferred by smart nanofluids. The concentration of nanoparticles needs to be tuned within a rather narrow range in order for the bistable behavior of the heat transferred to become apparent. Typical switching times between the conductive and convective stable states are of the order of a few hours. However, shorter transition times could in principle be obtained by mechanical manipulation of the sample, or by using external fields to achieve a more rapid redistribution of the nanoparticles.

ACKNOWLEDGMENTS

We thank R. Cerbino and G. Donzelli for inspiring discussion and comments to this work. We thank F. Finozzi for the measurements on water. We acknowledge the supply of the LUDOX sample from Grace Davison and of the HYFLON sample from R. Piazza.

[1] P. Keblinski, J. A. Eastman, and D. G. Cahill, Mater. Today **8**, 36 (2005).
[2] J. Buongiorno *et al.*, J. Appl. Phys. **106**, 094312 (2009).
[3] J. W. Gao, R. T. Zheng, H. Ohtani, D. S. Zhu, and G. Chen, Nano Lett. **9**, 4128 (2009).
[4] L. Godson, B. Raja, D. M. Lal, and S. Wongwises, Renew. Sust. Energy Rev. **14**, 629 (2010).
[5] V. I. Terekhov, S. V. Kalinina, and V. V. Lemanov, Thermophys. Aeromech. **17**, 1 (2010).
[6] V. I. Terekhov, S. V. Kalinina, and V. V. Lemanov, Thermophys. Aeromech. **17**, 157 (2010).
[7] S. Krishnamurthy, P. Bhattacharya, and P. E. Phelan, Nano Lett. **6**, 419 (2006).
[8] S. Ozturk, Y. A. Hassan, and V. M. Ugaz, Nano Lett. **10**, 665 (2010).
[9] J. Philip, P. D. Shima, and B. Raj, Appl. Phys. Lett. **92**, 043108 (2008).
[10] P. D. Shima, J. Philip, and B. Raj, Appl. Phys. Lett. **95**, 133112 (2009).
[11] G. Donzelli, R. Cerbino, and A. Vailati, Phys. Rev. Lett. **102**, 104503 (2009).
[12] S. Chandrasekhar, *Hydrodynamic and Hydromagnetic Stability* (Dover, New York, 1981).
[13] T. E. Faber, *Fluid Dynamics for Physicists* (Cambridge University Press, Cambridge, 1995).
[14] Ludox®TMA, Grace Davison. The particles have a diameter of 32 nm. Other properties of the sample at 30 °C are $D = 2.2 \times 10^{-7}$ cm^2/s, $\kappa = 1.52 \times 10^{-3}$ cm^2/s, $\alpha = 2.97 \times 10^{-4}$ K^{-1}, $\nu = 8.18 \times 10^{-3}$ cm^2/s, $\beta = 0.57$, $S_T = -4.7 \times 10^{-2}$ K^{-1}, and Le $= 6.49 \times 10^3$.
[15] A. Vailati and M. Giglio, Phys. Rev. Lett. **77**, 1484 (1996).
[16] A. Vailati and M. Giglio, Nature (London) **390**, 262 (1997).
[17] R. Cerbino, A. Vailati, and M. Giglio, Phys. Rev. E **66**, 055301 (2002).
[18] S. Mazzoni, R. Cerbino, D. Brogioli, A. Vailati, and M. Giglio, Eur. Phys. J. E **15**, 305 (2004).
[19] R. Cerbino, S. Mazzoni, A. Vailati, and M. Giglio, Phys. Rev. Lett. **94**, 064501 (2005).
[20] A. Vailati *et al.*, Appl. Opt. **45**, 2155 (2006).
[21] S. Mazzoni, F. Giavazzi, R. Cerbino, M. Giglio, and A. Vailati, Phys. Rev. Lett. **100**, 188104 (2008).
[22] F. Giavazzi and A. Vailati, Phys. Rev. E **80**, 015303 (2009).
[23] A. Vailati *et al.*, Nat. Commun. **2**, 290 (2011).
[24] Ferrotec, Thermoelectric Reference Guide, Mathematical Modeling of Modules, [http://thermal.ferrotec.com/technology/thermoelectric/thermalRef11/].
[25] R. P. Behringer and G. Ahlers, J. Fluid Mech. **125**, 219 (1982).
[26] A. Ryskin and H. Pleiner, Phys. Rev. E **71**, 056303 (2005).
[27] M. I. Shliomis and B. L. Smorodin, Phys. Rev. E **71**, 036312 (2005).
[28] V. M. Shevtsova, D. E. Melnikov, and J. C. Legros, Phys. Rev. E **73**, 047302 (2006).
[29] M. C. Kim and C. K. Choi, Phys. Rev. E **76**, 036302 (2007).
[30] M. C. Kim, C. K. Choi, and J.-K. Yeo, Phys. Fluids **19**, 084103 (2007).
[31] B. Huke, H. Pleiner, and M. Lücke, Phys. Rev. E **75**, 036203 (2007).
[32] R. Savino and D. Paterna, Phys. Fluids **20**, 017101 (2008).
[33] M. Gläßl, M. Hilt, and W. Zimmermann, Eur. Phys. J. E **32**, 265 (2010).
[34] B. Elhajjar, G. Bachir, A. Mojtabi, C. Fakih, and M. C. Charrier-Mojtabi, C. R. Mécanique **338**, 350 (2010).
[35] F. Winkel, S. Messlinger, W. Schöpf, I. Rehberg, M. Siebenbürger, and M. Ballauff, New J. Phys. **12**, 053003 (2010).
[36] M. Gläßl, M. Hilt, and W. Zimmermann, Phys. Rev. E **83**, 046315 (2011).
[37] M. C. Kim, Eur. Phys. J. E **34**, 27 (2011).
[38] B. L. Smorodin, I. N. Cherepanov, B. I. Myznikova, and M. I. Shliomis, Phys. Rev. E **84**, 026305 (2011).
[39] M. Giglio and A. Vendramini, Phys. Rev. Lett. **38**, 26 (1977).
[40] J. K. Platten and J. C. Legros, *Convection in Liquids* (Springer, Berlin, 1984).
[41] Hyflon®MFA, Solvay-Solexis. The particles have a diameter of 44 nm. Other properties of the sample at 25 °C are $D = 1.30 \times 10^{-7}$ cm^2/s, $\kappa = 1.47 \times 10^{-3}$ cm^2/s, $\alpha = 2.52 \times 10^{-4}$ K^{-1}, $\nu = 8.96 \times 10^{-3}$ cm^2/s, $\beta = 0.54$, and $S_T = -9.0 \times 10^{-2}$ K^{-1}.